CHAPTER 4

TSUNAMI DETECTION USING REMOTE SENSING TECHNIQUE

4.1 GENERAL

Waves are the ocean's most important features which transport energy from one place to other. Wavelengths can vary from few centimeters to hundreds of meters and wave heights may vary from tiny perturbation in ocean surface to tens of meters. Measuring the ocean waves from space is the key contribution towards the satellite remote sensing. If the wave attributes such as wavelength, wave height and direction of propagation can be found effectively, this information may recover our acceptance values towards the distinctive compelling towards the ocean.
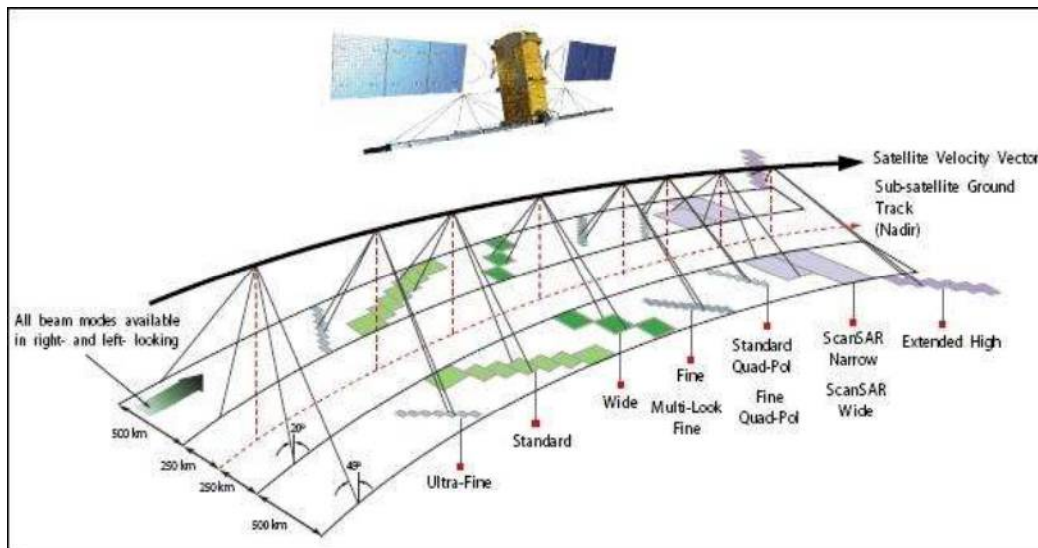
Figure 4.1   Schematic diagram for the different modes obtained by RADARSAT-2 sensor.

RADARSAT-2 is the Earth Observation Satellite (EOS) that was successfully launched on 14 December 2007 with the unique collaboration of the Canadian Space Agency (CSA) and the industry MacDonald, Dettwiler and Associated Ltd. (MDA), Canada. It carries a C-band (5.40 GHz) SAR instrument in order to achieve good resolution imageries. RADARSAT-2 has been designed with significant and powerful technical advancements that include high-resolution

imaging, left and right-looking imaging options, superior data storage and more precise measurements of spacecraft position and attitude.

Table 4.1 Imaging mode characteristics of RADARSAT-2.

Imaging Mode	Nominal swath [km]	Resolution (range x azimuth) [m]	Polarization	Incidence angle [°]
Standard	100	25 x 28	Quad	20 ~ 49
Wide	150	25 x 28	Quad	20 ~ 45
ScanSAR wide	500	100 x 100	Quad	20 ~ 49
ScanSAR narrow	300	50 x 50	Quad	20 ~ 47
Standard quad-polarization	25	25 x 28	Quad	20 ~ 41
Fine quad-polarization	25	11 x 9	Quad	20 ~ 41
Ultrafine	20	3 x 3	Quad	30 ~ 50

Figure 4.1 illustrates the imaging capabilities of RADARSAT-2 sensor which involves the different imaging modes of operation. Table 4.1 gives the specification of RADARSAT-2 sensor in terms of its imaging mode of operation, swath width, resolutions, polarizations and incidence angles. The satellite is placed over an altitude of approximately 792 *Km* above the earth surface.

4.2 WAVE IMAGING MECHANISMS

Wave modeling is significant method to produce the ocean waves under various wind conditions. Active wave representations are compelled by the wind turfs and could be initiated by the initial wind conditions using in-situ data and remotely sensed data. Remotely sensed data can be recycled to modify wind's early circumstances. RADAR/SAR is the unique sensor to observe the ocean and can deliver images from the interplanetary with extraordinary resolution. The fine-detail imagery of the ocean's surface from SAR is more complex. SAR provides the directional wave information. The radar backscatter is from baby undulations and the deceptive modulation of undulations with long waves can easily be seen in SAR images (Johnsen *et. al.*, 1999). The radar signals are extra exaggerated by variations in metrological circumstances such as the sea-state, wind speed and its directions (Caprari *et.al.*, 2000).

Various ocean surface phenomena that affect the amplitude or spectral distribution of these waves will be visible on the radar images (Vachon and Raney, 1991).

4.2.1 Bragg Resonance Phenomenon

SAR backscattering from the sea surface is within the incidence angle range of $18^0 \sim 50^0$ in absence of longwave. Bragg scattering phenomena is shown in Figure 4.2. Under the Bragg scattering, the incidence radar waves are backscattered by the wind-generated and short wave components of the ocean surface wavelength (λ_B), whose characteristics are same as of the radar wavelength (λ_r) and are given as,

$$\lambda_B = \frac{\lambda_r}{2\sin\theta} \tag{4.1}$$
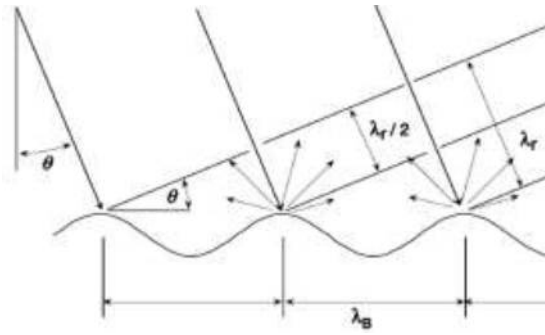
Figure 4.2 Illustration showing the Bragg scattering phenomena [adapted from *Martine*, 2004].

Brown *et.al.*, (1977) proposed some of the tools which correlate the SAR-ocean image formation. The standard expression of the radar reflectivity or brightness can be written as,

$$\sigma^0 = 10\log_{10}\left(\frac{\sigma}{S}\right) \tag{4.2}$$

where σ is the scattered energy sensed by the antenna over a specified area S, σ^0 is the Normalized Radar Cross-Section (NRCS).

For radars, the RCS is related to the ocean surface unevenness at various radar wavelengths. Wright (1968) defined the radar cross section for the perfectly conducting ocean surface as,

$$\sigma^0 = 16\pi k_0 \left(1 \pm \sin^2\theta\right) \zeta\left(2k_0\sin\theta\right) \tag{4.3}$$

where k_0 is the radar wave number, ζ is the wave spectra, "plus" sign relates for the VV polarization and "minus" sign for the HH polarization, θ is the incidence angle. The SAR imaging tool is intrinsically related to how SAR can create the radar image for the ocean surfaces.

4.2.2 Modulation Transfer Function (MTF)

There are three primary mechanisms by which longwave modify the Bragg waves to affect the SAR imaging. The basic theory was proposed by Alpers *et*. *al*., (1983).
(i) Tilt Modulation
(ii) Hydrodynamic Modulation
(iii) Velocity Bunching Modulation

(i) Tilt Modulation

As the longwave propagate towards the shortwave field region, adjustment in the shortwaves is made which directly changes the intensity and thus the radar imaging. Tilt modulation occurs when the varying slope of longwaves changes with the local orientation or tilt of the shortwaves. These tilting waves act as the reflecting mirrors or facets to radar incidence waves, this energy is only seen by the radar to form an image of the ocean surface. The process simply returns a stronger echo from those parts of the wave surface profile facing towards the radar than those away**.** The tilt modulation function can be expressed as:

$$T_k^{tilt} = -4ik_y \frac{\cot\theta}{1+\sin^2\theta} \tag{4.4}$$

(ii) Hydrodynamic Modulation

Keller and Wright (1975) first gave the definition of the hydrodynamic modulation, wherein the hydrodynamic contact between longwave and capillary waves causes the deviation and conjunction and modulate the returned energy. The process relies on the fact that small-scale (centimeter-decimeter wavelength) ripples control the magnitude of radar echo through the Bragg mechanism when the radar points obliquely to the surface. This fluctuating dissemination could be caused by the change in the local angle of tilt of the long and short waves. The hydrodynamic modulation function can be expressed with the following relationship:

$$T_k^{hydr} = -4.5\omega \frac{k_y^2(\omega - i\chi)}{|k_0|(\omega^2 + \chi^2)} \qquad (4.5)$$

(iii) Velocity Bunching Modulation

Velocity bunching mechanism is a consequence of the fine-known consequence of azimuth image swing *i.e.*, the pixel of a range moving targets (direction perpendicular to the flight path) is shifted in azimuth by an quantity relative to the velocity (Valenzuela, 1978 and Ouchi, 1984). If the shorter waves have a non-uniform distribution of the slant-range velocity components, the images of the waves are moved non-uniformly and the complete pixels would be modulated. The velocity bunching modulation function can be expressed as:

$$T_k^{rb} = -ik_y \frac{\cos\theta}{\sin\theta} \qquad (4.6)$$

The modulation transfer function (MTF) can be expressed as the summation of all three transfer functions. $T(k_0)$ is the modulation transfer function which describes the charting of ocean surface wave bands into the radar image bands. It can be expressed as follows,

$$T(k_0) = T_k^{tilt} + T_k^{hydr} + T_k^{rb} \qquad (4.7)$$

where k_0, k_y, θ, χ, and ω represents the resultant wave number, azimuth wave number, incidence angle, permeability of sea surface and wave angular frequency respectively.

In opinion, the correlation between observed radar image intensity-variance spectrum, $S_I(k_0)$, and the ocean surface wave height-variance spectrum, $\zeta(k_0)$, is known by,

$$S_I(k_0) = T(k_0)\zeta(k_0) \qquad (4.8)$$

4.3 DATASET DESCRIPTION

Approaches used to detect the tsunami indication have been labeled before. Here in this investigation we define and validate a recognition procedure based on the various annotations. In order to review the statement methodologies: (i) radar ranges (4-*minutes* resolution time) are examined to provide radial speeds; (ii) radial speeds in the area bands 2*Km* width and about

equivalent to depth shapes measured in the course vertical to the depth shape and aiming to coast; (*c*) These speed mechanisms are considered over various bands datasets (*d*) the periodic signal of typical speed in respective radar band dataset is designed, which displays an individual fluctuations twisted by tsunami waves signal function.
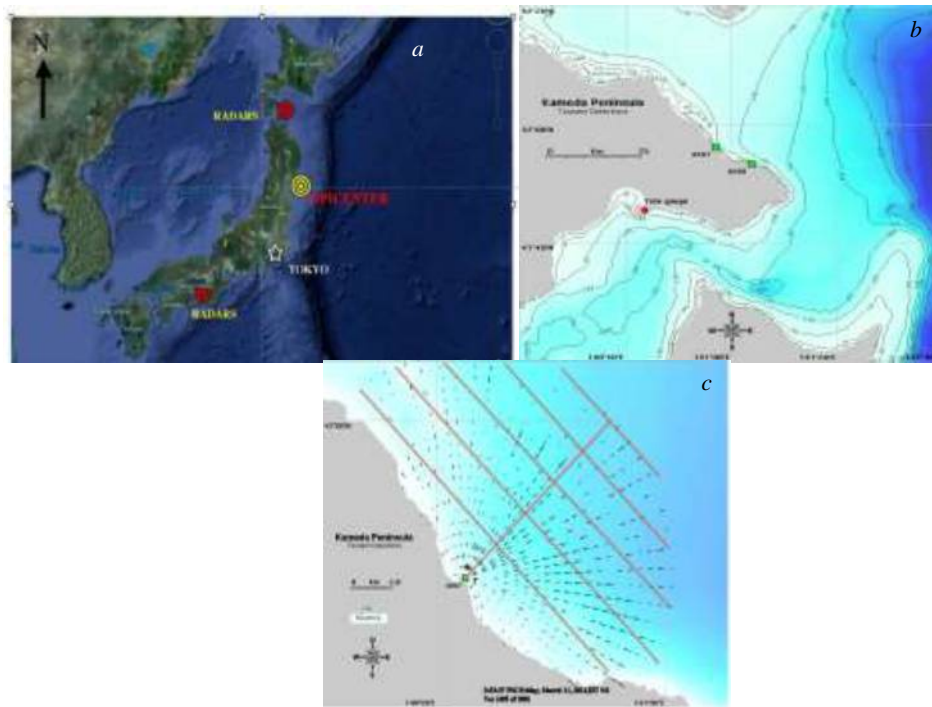
Figure 4.3 (*a*) The universal site of the Japan earthquake and the radars in Hokkaido and on the Kii Strait. (*b*) The bathymetry offshore Kameda Peninsula, (*c*) Circular current speeds from the, Hokkaido radar.

Figure 4.3 *a-b* represents the region of the tools in Japan that formed the data utilized in the present study. Two radars on the Kameda Peninsula, two radars on the Kii channel and neighboring tide/wave gauges. Also displayed is the offshore bathymetry.

Figure 4.3 *c* contributes an example of dignified 4*minutes* circular vectors, the 2*Km* area bands used in this study. For the usage in dispensation for wave's speeds, numerous spectra are averaged for the various times. For the tsunami detection, wave spectra are cast-off to exploit the subsequent resolution period. The averaged velocity constituent detected at Hokkaido, for three 2*Km* bands fluctuating from 7-13 *Km* away from the coast. Radar operational frequency is taken as 47*MHz* for this experiment.

4.4 METHODOLOGY

Here in this research, we have tried to formulate the equation of arrival of tsunami from deep ocean to the coastal line based on the *q*-factor (**Lipa *et.al.*, 2011**). At a particular time,*t,* a tsunami detection factor (*q*-factor) is defined for which signals the tsunami arrival when it exceeds a present threshold. The detailed methodology for the q-factor estimation is as shown in Figure 4.4.
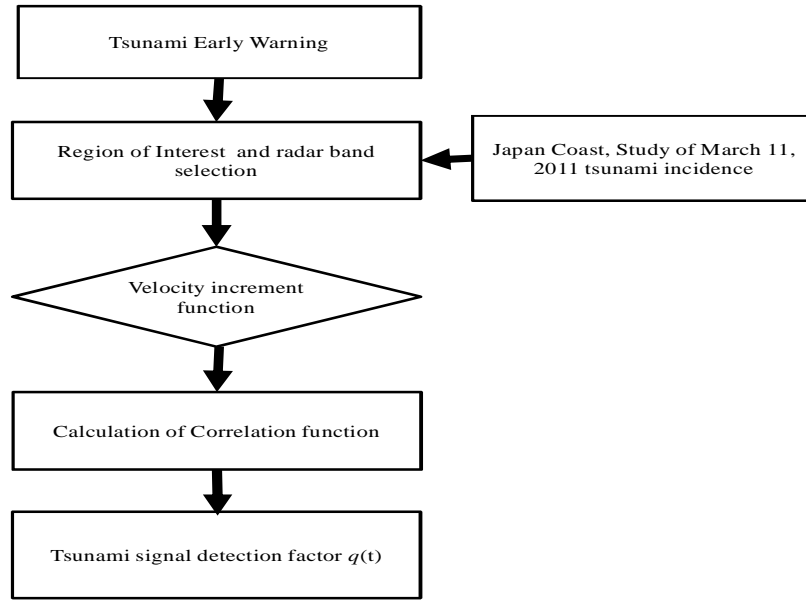
Figure 4.4 Flow chart for the tsunami detection factor (*q*-factor) measurement using radar remote sensing technique.

Velocities at three adjacent time intervals and three region bands are inspected for relationships as follows:

(i) At time *t*, for band *b* compute the average value $a_b(t)$ and the standard deviation $s_b(t)$ above the earlier hour.

(ii) In each band, estimate a degree of the velocity deviation

$$d_b(t) = \left[\frac{v_b(t) - a_b(t)}{s_b(t)} \right] \tag{4.9}$$

(iii) The velocity deviation function is defined as,

$$D(t) = \prod_b d_b(t) \tag{4.10}$$

In each band, analyze the transformation in velocity above two end-to-end time intermissions from $t - 2\delta$ to t, where δ is time difference of the input datasets:

$$\Delta v_b(t) = v_b(t) - v_b(t - 2\delta) \tag{4.11}$$

Velocity increment function $\Delta V(t)$ is defined to be the sum over the bands:

$$\Delta V(t) = \sum_b \Delta v_b(t) \tag{4.12}$$

(iv) Compute a correlation function $C(t)$ labeling the connection between speeds in all three end-to-end bands over times $t, t - \delta, t - 2\delta$, where δ is the time resolution of the input data.

(v) q-factor for the time t is examined as,

$$q(t) = D(t)C(t)\Delta V(t) \tag{4.13}$$

4.5 q-FACTOR MEASUREMENT USING RADAR REMOTE SENSING APPROACH

Figure 4.4 expresses the velocities in six 2Km zone bands calculates by, Hokkaido (A088) radar and the equivalent q-factors (Lipa *et.al.*,2011). The tsunami reaches after an hour afterward an earthquake occurs, as specified by the association in speeds for dissimilar radar bands. This concludes to the sudden rise in the q-factor, representing tsunami onset. Tsunami signals are mostly strong in these bands additional in correlation to radars, earlier to coast flow of current is unfocused similar to coast, sinking of the vertical graphs plotted. This radar functions for 40 minutes in an hour, causing in the 20minutes gaps noticeable in the plots. The depth of water level is much smaller than 60m above the overall radar reporting zone. The influx of the tsunami wave is designated by relationship among speeds in dissimilar radar bands opening after 2.5h afterwards the tsunami. The usual process for manipulating the speed deviance influence was nullified by period slits in the characteristics of input statistics. The simulation has been carried out with the reference of equation 4.13.

The q-factor demonstrates unexpected change in size is about 8 minutes afterward the shock of velocity relationships. At this stage, the speed reduces, representing that the tsunami is touching off to the coast, causing in the destructive sharp q-factor as resulted in Figure 4.5 (d). The negative q-factor of for the tsunami signal starts after 2h of the tsunami influence. It can be decided that, there is an unchanging pattern for the feature before influx of tsunami waves.
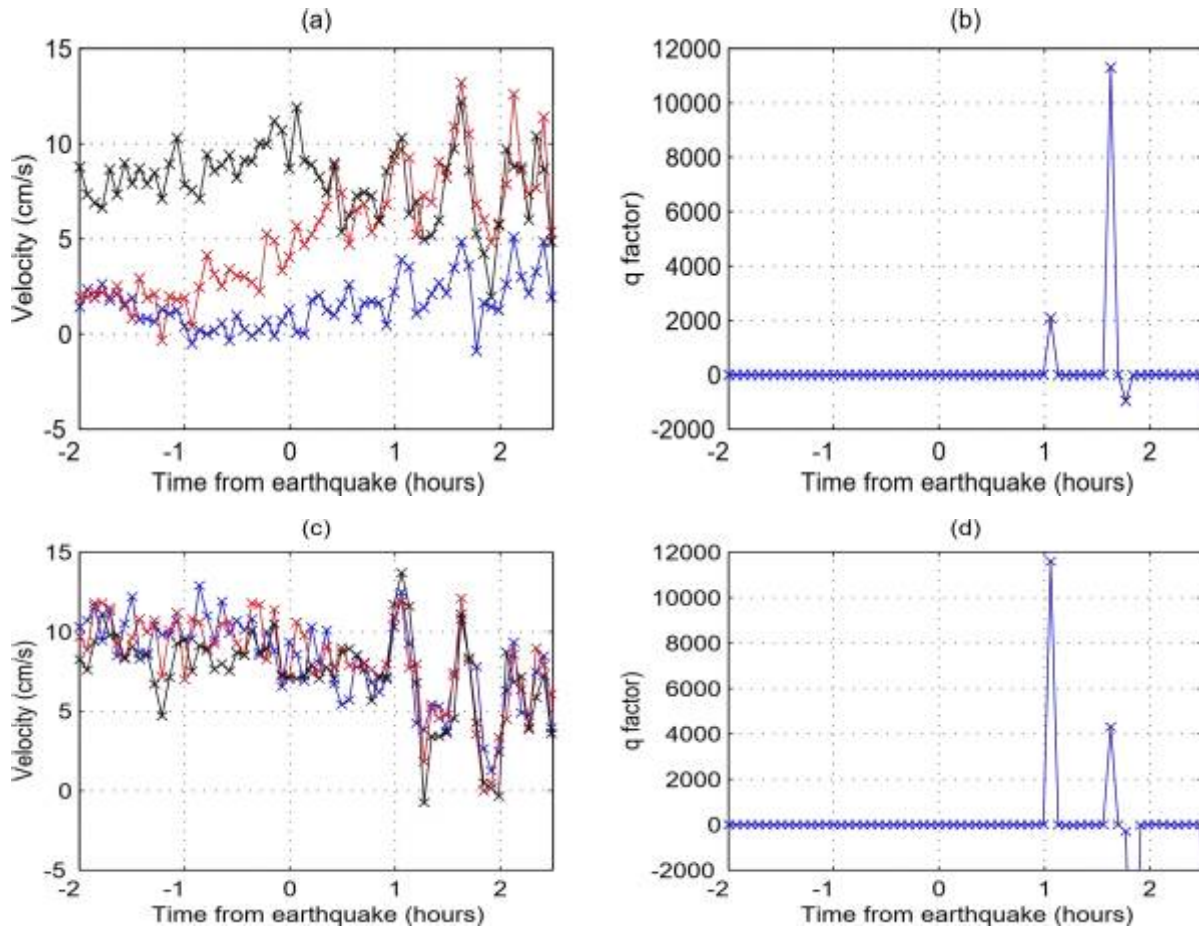
Figure 4.5 Time series of velocity components from radar A088. (**a**) Blue: 0–2 km; Red: 2–4 km; Black: 4–6 km over 5 h (**b**) *q*-factor for 0–6 km offshore (**c**) Blue: 6–8 km; Red: 8–10 km; Black: 10–12 km (**d**) *q*-factor for 6–12 km offshore [Lipa *et.al.*, 2011].

4.6 SUMMARY

RADAR remote sensing of ocean has been proposed in this chapter. Here in this chapter we have tried to formulate the equation of arrival of tsunami from Deep Ocean to the coastal line based on the *q*-factor. The tsunami detection function directly depends on the amount of microwave signals propagation towards the deep ocean where the tsunami used to arrive. The *q*-factor illustrates an abrupt change in scale about 8 *minutes* after the start of the velocity associations. At this point, the velocity is declining, representing that the tsunami is touching offshore, causing in the negative *q*-factor and reaches to the suitable significant description. The calculation of tsunami signal factor is determined using the time sequence of the velocity mechanisms from radar A088 located at the coast of Japan.